# Diffuse magnetic neutron scattering in the highly frustrated double perovskite Ba_{2}YRuO_{6}

Gøran. J. Nilsen, Corey M. Thompson, Georg Ehlers, Casey A. Marjerrison, and John E. Greedan

Phys. Rev. B **91**, 054415 — Published 23 February 2015

DOI: 10.1103/PhysRevB.91.054415

# Diffuse Magnetic Neutron Scattering in the Highly Frustrated Double Perovskite $Ba_2YRuO_6$

Gøran. J. Nilsen,[1,*] Corey M. Thompson,[2] Georg Ehlers,[3] Casey A. Marjerrison,[4] and John E. Greedan[2]

[1] *Institut Laue-Langevin, 6 rue Jules Horowitz, 38042 Grenoble, France*
[2] *Department of Chemistry and Chemical Biology and the Brockhouse Institute for Materials Research, McMaster University, Hamilton, Canada*
[3] *Oak Ridge National Laboratory, Oak Ridge, Tennessee, USA*
[4] *Department of Physics and Astronomy, McMaster University, Hamilton, Canada*

(Dated: January 12, 2015)

Diffuse magnetic scattering in the highly frustrated double perovskite, $Ba_2YRuO_6$, was investigated using polarized neutrons. Consistent with previous reports, the material shows two apparent transitions at 47 K and 36 K to an eventual Type I face centered cubic magnetic ground state. The (100) magnetic reflection shows different behavior from the five other observed reflections upon heating from 1.8 K, with the former broadening well beyond the resolution limit near 36 K. Closer examination of the latter group reveals also a small, but clear, increase in peak widths between 36 K and 47 K, indicating that this regime is dominated by short range spin correlations. Diffuse magnetic scattering persists above 47 K near the position of (100) to at least 200 K, consistent with strong frustration. Reverse Monte Carlo (RMC) modeling of the diffuse scattering from 45 K to 200 K finds that the spin-spin correlations between nearest and next nearest neighbors are antiferromagnetic and ferromagnetic, respectively, at temperatures near the upper ordering temperature, but both become antiferromagnetic and of similar magnitude above 100 K. The significance of this is unusual crossover is discussed in light of the super-super exchange interactions between nearest and next nearest neighbors in this material and the demands of the Type I order. The dimensionality of the correlations are addressed by reconstructing the scattering in the $(hk0)$ plane using the RMC spin configurations. This indicates 1D spin correlations dominate at temperatures close to the first transition. In addition, a comparison between mean field calculations and the $(hk0)$ scattering implies that further neighbor couplings play a significant role in the selection of the ground state. The results and interpretation are compared with those recently published for monoclinic $Sr_2YRuO_6$ and similarities and differences are emphasized.

PACS numbers: check

Double perovskite oxides with rock-salt ordering on the B-site (Fig. 1a) provide many opportunities for the design of new materials with geometric magnetic frustration. Such materials have the general composition $AA'BB'O_6$, where $A$ and $A'$ are large cations from Group 2 (Ca,Sr or Ba) or Group 3 (La and other large rare earth ions) and $B$ and $B'$ typically are smaller cations from the $3d$, $4d$ and $5d$ transition series, but can also include smaller ions from Groups 2 and 3 such as Mg, Zn, Ca and Y. The robustness of the perovskite structure allows a large variety of oxidation states and electronic structures. Geometric magnetic frustration arises when $B$ is a diamagnetic ion and $B'$ is magnetic; in this case, each forms a face centered cubic (fcc) sublattice, which is equivalent to a network of edge-sharing tetrahedra. In the presence of antiferromagnetic nearest-neighbor correlations such a lattice exhibits frustration, as seen in Figure 1b.

The symmetry of the lattice and the local point symmetry at the B′ site are determined by Goldschmidts tolerance factor, $t = (r_A - r_O)/\sqrt{2}(\langle r_B, r'_B\rangle - r_O)$, where $r_A - r_O$ and $\langle r_B, r'_B\rangle - r_O$ are the relevant cation-oxide ion distances[1]. As $t$ decreases from the ideal value of 1, space group symmetries $Fm\bar{3}m$, $I4/m$ and $P2_1/n$ are observed sequentially, with respective B′ site point symmetries of $m\bar{3}m$, $4/m$ and $\bar{1}$[2]. The point symmetries naturally determine the crystal field splitting of the $t_{2g}^n$ ground states. The B′ site electronic configuration confers a nominal spin, $S$, which can be strongly modified by spin orbit coupling (SOC), particularly when the B′ ion is from the $4d$ or $5d$ series. All of these factors – sublattice symmetry, point symmetry, $S$ and SOC – are "degrees of freedom" which sometimes play a major role in the determination of the magnetic ground state. Recent theory has attempted to take these factors in to account at the mean field level for the cases of configurations $t_{2g}^1$ and $t_{2g}^2$ for both $m\bar{3}m$ and $\bar{1}$ site symmetries with strong SOC[3–5].

The role of SOC is thought to be least important in the case where B′ has the $t_{2g}^3$ configuration, as to first order $L = 0$. Assuming $LS$ coupling the main effect arises at second order, and results in an isotropic reduction of the electronic $g$-factor by $\sim 8\lambda/10Dq$, where $\lambda$ is the spin orbit coupling constant and $10Dq$ is the overall cubic crystal field splitting between the $t_{2g}$ and $e_g$ states[6]. Thus, one expects that the ordered moment for $t_{2g}^3$ ions, $\mu_o = gS$, with S = 3/2 will be somewhat reduced from the spin only value of $3\mu_B$. For the case of interest here, namely $Ru^{5+}$ ($4d^3$), an estimated free ion value of $\lambda = 55$ meV[7] and $10Dq$ in the range $2 - 3$ eV indicates ordered moments should fall between $\mu_o \sim 2.7 - 2.8\ \mu_B$. Among other effects that can reduce the ordered moment is the strong covalency between the $4d$ and lig-

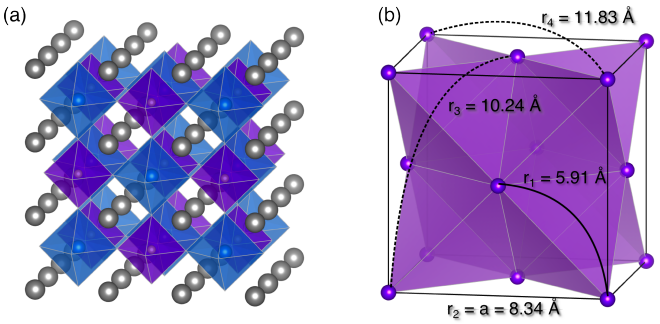


FIG. 1. (a) The crystal structure of the B-site ordered double perovskite, $A_2BB'O_6$. The grey spheres, purple octahedra and dark blue octahedra represent $A$ ions, $BO_6$ octahedra, and $B'O_6$ octahedra, respectively. (b) The geometrically frustrated face- centered-cubic lattice of edge-sharing tetrahedra formed by both the $B$ and $B'$ sites. Solid and dashed black lines indicate nearest-neighbor and next-nearest-neighbor Ru-Ru distances for $Ba_2YRuO_6$.

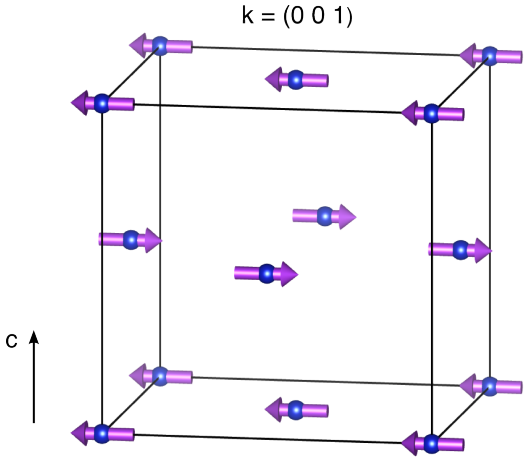


FIG. 2. The Type I fcc magnetic structure found for $Ba_2YRuO_6$ and several other $Ru^{5+}$ based double perovskites. The chosen moment direction is arbitrary as this cannot be determined from powder data on a material with cubic symmetry.

and orbitals, which removes some fraction of the moment from the metal ion site to the ligand sites. This is often considered to be the most important contribution to a reduced moment[8,9], but is difficult to quantify without detailed calculations of the electronic structure. Geometric frustration is also often invoked in the context of persistence of spin fluctuations to very low temperatures, but is even more difficult to quantify. Ordered moments for a number of $Ru^{5+}$ based double perovskites, namely $Ba_2YRuO_6$ and $Ba_2LuRuO_6$ which are cubic and $Sr_2LuRuO_6$, $Sr_2YRuO_6$ and $La_2LiRuO_6$ which are monoclinic, have been reported[10–12] and these span a very narrow range from 2.2(2) to 1.96(2)$\mu_B$. All of these $Ru^{5+}$ double perovkites show a Type I fcc ground state magnetic structure, pictured in Figure 2. Thus, there is a large ($> 30\%$) reduction in the $Ru^{5+}$ ordered moment from the spin only value. A similar moment reduction was found for the simple perovskite $SrTcO_3$, where the $Tc^{4+}$ ion has the same $4d$, $t_{2g}^3$ configuration and a moment of 1.9 $\mu_B$[8]. In this case, it was argued from a first principles calculation that most of the moment reduction arises from $4d$/ligand covalency[9,13]. Nonetheless, very recently, it has been suggested that SOC does play a major role in the magnetism of $4d^3$ and $5d^3$ perovskites in that a coupling scheme intermediate between $L-S$ and $j-j$ is appropriate for such a configuration[14]. So, the role of SOC in $4d^3$ and $5d^3$ perovskite magnetic materials appears to be unsettled, at least regarding moment reduction, at present.

However, seemingly unequivocal experimental evidence for the effects of SOC is provided by inelastic neutron scattering studies of the material with which this study is concerned, $Ba_2YRuO_6$[15]. A clear gap in the excitation spectrum, centered at the (001) antiferromagnetic zone center of 5 meV is seen. Such a gap is not expected for a pure $L = 0$ magnetic ground state. Bulk susceptibility studies on $Ba_2YRuO_6$ established the presence of two susceptibility maxima, at $T_{N2} \sim 36$ K and $T_{N1} \sim 47$ K[12]. Neutron diffraction (without energy analysis) and heat capacity data seemed to suggest that true ordering occurs only at the lower temperature; diffuse magnetic scattering was seen to persist up to at least $\sim 40$ K in the form of a broad, apparently symmetric feature at the (100) peak position $Q_{100} = 0.75$ Å$^{-1}$, but these studies were not pursued to higher temperatures. However, later neutron scattering studies including energy analysis, demonstrated that the (100) and (110) magnetic reflections remained resolution limited up to 47 K with a low incident energy and a narrow energy analysis window[15]. Upon widening the energy analysis window, the data more closely resembled those of the original diffraction experiments. At this point it was deemed useful to carry out experiments with polarized neutrons to examine the scattering above $T_{N2}$ in greater detail and to illuminate further the unusual magnetic ordering process in this double perovskite.

At about the time that these experiments were undertaken, a detailed neutron study of the related, but not isostructural, compound $Sr_2YRuO_6$ appeared[16]. $Sr_2YRuO_6$ is monoclinic, crystallizing in space group $P2_1/n$, while $Ba_2YRuO_6$ within the resolution of present measurements appears to remain $Fm\bar{3}m$ to the lowest temperatures studied. Nonetheless, the properties of the two compounds are very similar. $Sr_2YRuO_6$ exhibits two apparent transitions from specific heat and susceptibility data at $T_{N2} \sim 27$ K and $T_{N1} \sim 32$ K[17]. Prior neutron diffraction studies had confirmed the Type I fcc magnetic structure with the moments ferromagnetically aligned in the {001} planes and stacked antiferromagnetically along the propagation vector $\mathbf{k} = (001)$[10].

The investigation described in Ref. 16 consisted of a standard structural refinement and a more detailed study in a limited $Q$ window $0.35 < Q < 1.4$ Å$^{-1}$ using a triple

TABLE I. Comparison of the observed and calculated positions for six magnetic reflections for $Ba_2YRuO_6$ at 1.8 K.

| $(hkl)$ | $Q_{calc}$ / Å$^{-1}$ | $Q_{obs}$ / Å$^{-1}$ |
|---|---|---|
| 100 | 0.7548 | 0.756(1) |
| 110 | 1.0675 | 1.0690(5) |
| 210 | 1.6878 | 1.6839(8) |
| 211 | 1.8940 | 1.896(3) |
| 300 | 2.2645 | 2.256(3) |
| 310 | 2.3870 | 2.386(2) |

axis spectrometer in the double axis mode, *i.e.*, without energy analysis. Within this $Q$-range only two magnetic reflections were observed, (001) and (110). Among the remarkable findings were the observations that at 36 K, above $T_{N1}$, the (001) magnetic reflection took on an asymmetric shape and that this diffuse scattering persisted up to $\sim$ 200 K, more than six times $T_{N2}$. The lineshape was interpreted as Warren-like, arising from $2D$ correlated domains, and assigned to the presence of antiferromagnetically coupled ferromagnetic layers, a natural interpretation given the layered nature of the Type I structure. As well, the temperature dependence of the (110) reflection showed a change in slope between $T_{N2}$ and $T_{N1}$. However, the temperature dependence of (001) was not shown. It was also suggested that within the region $T_{N2} < T < T_{N1}$, long range order of alternate AFM layers occurs, and that this pattern of ordering should be general for nearly all fcc magnetic lattices. Another interesting observation concerned the strong increase in integrated magnetic scattering with increasing temperature, peaking at $\sim$ 33 K, just above $T_{N1}$, and then falling significantly with further heating to 200K. Finally, it was stated that for double perovskites in general that the next nearest neighbor (nnn) magnetic interaction, a 180∘ Ru-O-Y-O-Ru super-super exchange is negligible in comparison to the nearest neighbor (nn), 90′ interaction, which could have both Ru-Ru direct and Ru-O-Y-O-Ru components. This provided another strong motivation to complete a similar study on the closely related material, $Ba_2YRuO_6$. In the present work, polarized neutrons are used to explore a wider $Q$ range, $0.4 < Q < 3.9$ Å$^{-1}$ over a similarly broad temperature range up to 200 K. The diffuse scattering data is analyzed using reverse Monte-Carlo methods, which do not involve the choice of a lineshape model, as will prove important to the interpretation of the nature of the correlations. Finally, the signs of nn and further-neighbor exchanges are investigated by comparing the reconstructed single-crystal scattering calculated with a mean field model including exchanges up to fourth neighbors.

## I. EXPERIMENTAL

A $\sim$ 15 g sample of $Ba_2YRuO_6$ was prepared as described in a previous publication[12]. Analysis by x-ray powder diffraction showed a single phase product with a unit cell constant identical within statistical error with that reported. This sample is from the same batch as used in the inelastic neutron scattering experiments described previously[15]. A polarized neutron scattering experiment was carried out on the diffuse scattering spectrometer D7 at the ILL. The incident wavelength and energy were 3.12 Å and 8.97 meV, respectively, and the elastic $Q$-range covered was $0.4 < Q < 3.9$ Å$^{-1}$ . No energy analysis was carried out, meaning that the scattering was integrated between energy transfers $\sim -20$ meV$<$ $E < 8.4$ meV. The total cross section was separated into magnetic, spin incoherent, and nuclear/isotope incoherent components using the XYZ method detailed in[18,19]. Data from spin flip and non-spin flip separations of the magnetic cross section were combined to form an average magnetic scattering cross section, $(d\sigma/d\Omega)_{mag}$. Finally, a normalization to vanadium data was performed to allow for conversion to absolute units.

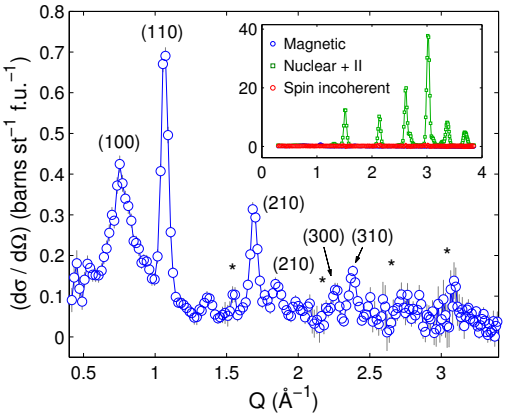


FIG. 3. Magnetic scattering after separation from other scattering contributions for $Ba_2YRuO_6$ at 35.8 K, showing the broadened (100) and relatively sharp (110), (210), (211), (300) and (310) magnetic reflections. The asterisks indicate the positions the four strongest nuclear Bragg peaks (see inset), which generate small anomalies in the magnetic cross section. The apparent peak at $\sim$ 1.3 Å$^{-1}$ is probably spurious, as it has no systematic temperature dependence. (inset) The separation of the cross section into its magnetic (blue), spin incoherent (red), and nuclear and isotope incoherent (II) (green) components by XYZ polarization analysis.

## II. RESULTS AND DISCUSSION

### A. T=1.8-44.8 K

Six reflections which are consistent with the Type I fcc magnetic structure reported previously for this material could be indexed unambiguously. The peak positions are shown in Table 1 for 1.8 K and are compared with those expected using the lattice parameter $a = 8.3259(5)$ Å at 4 K measured previously[12]. The temperature dependence of the integrated intensity of the (100) magnetic

reflection is essentially the same as that reported, *i.e.*, it is consistent with $T_{N2} \sim 36$ K [see Figure 4a]. However, at higher temperatures, the (100) reflection broadens significantly in $Q$, while the (110) and (210) reflections remain resolution-limited and Gaussian-like, as illustrated in Figures 3 and 4a.

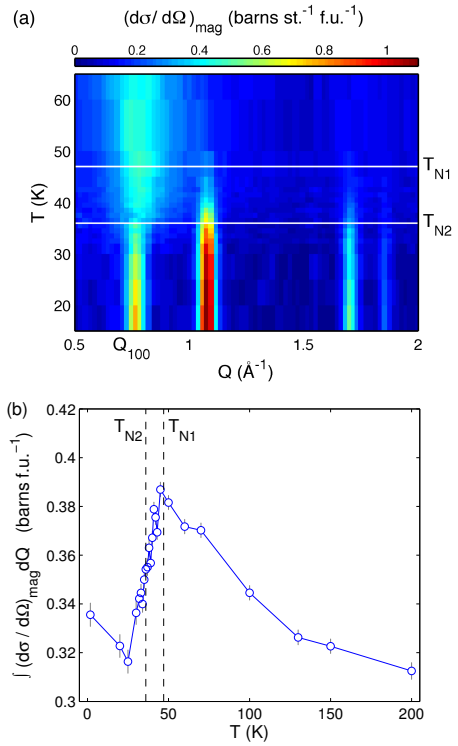


FIG. 4. (a) The temperature- and Q-dependence of the magnetic scattering on passing through $T_{N1}$ and $T_{N2}$, indicated by white lines. (b) The integrated total magnetic cross section at various temperatures for $Ba_2YRuO_6$. A sharp drop is observed at $T_{N1}$, resulting from the opening of the gap.

The temperature dependence of the intensities and widths of the two strongest of these, the (110) and (210) reflections, are shown in Figure 5a. Note that both show order parameter-like behavior upon approaching $T_{N2}$ from lower temperatures, but a much more gradual decrease above $T_{N2}$. This is similar to the behavior of the (110) reflection reported for $Sr_2YRuO_6$.[16] We note that neither the (110) nor the (210) reflections were observed above $T_{N2} = 36$ K in the previous study of $Ba_2YRuO_6$ using diffraction methods[12]. It is also clear that the widths of both peaks increase significantly beyond the resolution $\Delta Q \sim 0.05$ Å$^{-1}$ above $T_{N2}$, indicating that the region between $T_{N2}$ and $T_{N1}$ does not represent true long range order but that correlations of finite dimension are present [Figure 5b]. The resolution-deconvoluted correlation lengths found in this region decrease smoothly from $\xi = 63(22)$ Å at 35 K to 19(9) Å at 45 K. Thus, we establish that $T_{N2} = 36$ K is the true critical temperature for this material.

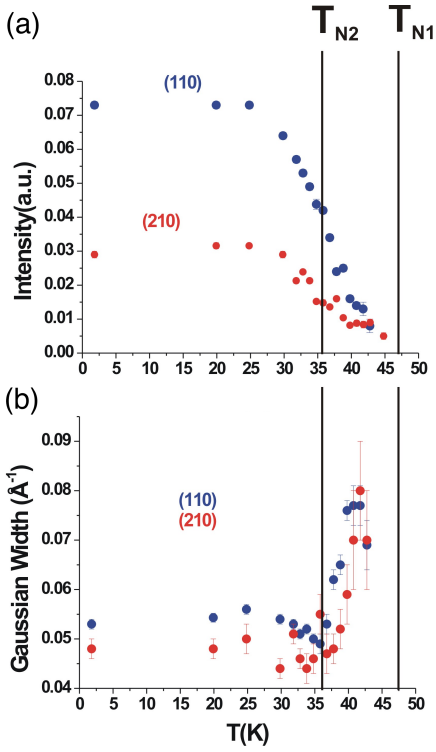


FIG. 5. The temperature dependence of the intensities (a) and Gaussian widths (b) of the (110) and (210) magnetic reflections for $Ba_2YRuO_6$. The vertical lines locate $T_{N2}$ and $T_{N1}$. Note the order parameter-like behavior for the intensities below $T_{N2}$ and the more gradual decrease between $T_{N2}$ and $T_{N1}$. While both reflections broaden significantly above $T_{N2}$, the Gaussian (resolution) component remains dominant, making a Gaussian a good approximation of the line-shape.

### B. T=49.8-200 K

Above 50 K the only surviving magnetic feature is a very broad peak near $Q_{100} = 0.75$ Å$^{-1}$ [Figure 4a]. Remarkably, the peak persists up to 200 K, as in $Sr_2YRuO_6$, indicating the presence of short range magnetic correlations to at least $6T_{N2}$. This is direct evidence for the high level of frustration in these fcc lattice magnetic materials. In the case of $Sr_2YRuO_6$, the peak shape is interpreted as Warren-like[16], while for $Ba_2YRuO_6$ the dimensionality of correlations is less obvious to assign; indeed, it is possible to fit the peak using either an asymmetric 2D Warren or a symmetric 3D Lorentzian lineshape function. Matters are complicated by the presence of quasi-elastic critical scattering around $Q_{100}$ at high temperature, which has already been shown to have a highly asymmetric lineshape[15].

The $T > 40$ K data from D7 clearly contains a significant contribution from this inelastic scattering, given the absence of energy analysis. We do not, however, expect a significant distortion of our measured cross-section to result from the inelasticity because *(i)* the inelastic intensity is concentrated in a single rod of scattering at

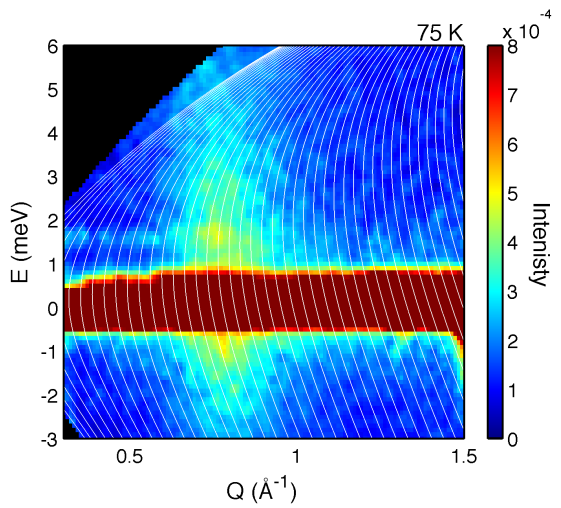


FIG. 6. $S(Q,E)$ measured at 75 K from [15]. The detector trajectories integrated over in our polarized scattering experiments are indicated by white lines. The color scale is normalized to the magnetic intensity at $Q_(100)$ and $E = 0$.

$Q_{100}$, and *(ii)* the spectral weight at low energy transfer $E < 2$ meV is much greater than at higher energies. We show this by plotting the $(Q,E)$ trajectories of the D7 detectors over the 75 K data from [15] in figure 6; around $Q_{100}$, a slight broadening on the low $Q$ side accompanied by a higher background is expected, an effect which decreases with the reduction in inelastic scattering upon cooling. Furthermore, the scattering above the gap energy in the low $T$ gapped phase should be confined to the first few detectors in the lowest angle bank, meaning that the observed pattern represents a clean separation of elastic and inelastic magnetic scattering. With the above in mind, a choice has been made to analyze the total measured diffuse scattering profile using reverse Monte Carlo methods, which do not involve an analytical model for the lineshape or a priori assumptions about dimensionality. These results are described in the following section.

Further evidence of the influence of the inelastic gap is shown in figure 4b where the integrated magnetic cross section over the full instrumental Q-range is displayed as a function of temperature. Note several features; *(i)* the total scattering increases upon cooling towards $T_{N1}$ *(ii)* At $T_{N1}$, it sharply decreases and continues doing so beyond $T_{N2}$, where *(iii)* the total scattering eventually increases again. The sharp decrease at $T_{N1}$ is consistent with the opening of a gap, which has already been observed in inelastic neutron scattering experiments[15], while the increase at lower temperature reflects the growth of the magnetic Bragg peaks.

The overall temperature dependence mirrors that of $Sr_2YRuO_6$, where the apparent decrease in the total scattering below $T_{N1}$ was not provided with an explanation[16]. Given the inelastic data in[15], however, we believe that $Sr_2YRuO_6$ should also be a gapped system. Finally, given that the cross sections obtained from D7 data are in absolute units, and because the gap exceeds the energy window of our neutron scattering experiment, it is possible to derive the model-independent ordered magnetic moment from the data at $T = 1.8$ K by comparing the total scattering with the integral of

$$\left(\frac{d\sigma}{d\Omega}\right)_{mag} = \frac{2}{3}(\gamma r_0)^2 \left[\frac{1}{2} g f(Q)\right]^2 S^2 \qquad (1)$$

over all $Q$, where $f(Q)$ is the magnetic form factor and the constants have their usual definitions, which assumes that the measured scattering is dominated by the ordered component. Using $f(Q)$ for $Ru^{5+}$ from[20], the resulting moment at 1.8 K is $\mu_o = 2.05(4)\ \mu_B$, in excellent agreement with the value $2.11(6)\ \mu_B$ derived from neutron diffraction data[11,12].

### C. Reverse Monte Carlo fits

As already pointed out RMC analysis of the existing data sets are more appropriate than fitting to analytic functions and can provide new information, especially regarding direct space spin-spin correlations up to well beyond nearest neighbor distances. Such methods have been applied recently to a number of disordered magnetic systems[21,22]. Two different RMC codes were applied, a locally developed one that had been used in the case of the highly frustrated pyrochlore $Tb_2Mo_2O_7$[21] and the SPINVERT program which has recently become widely available[22,23]. There was good agreement between the two methods with only slight differences as discussed in Appendix 1. The results from the SPINVERT code will be used in the following. The box sizes used were $14 \times 14 \times 14$ (10976 spins), and convergence was typically reached within $200 - 500$ moves per spin. To approximate the $Ru^{5+}$ form factor, which is not tabulated, we attempted several approximations: *(i)* using the estimated $Ru^{5+}$ $f(Q)$ from [20] (ii) $f(Q)$ for the isoelectronic $5d$ ion $Os^{5+}$[24] (iii) and $f(Q)$ for the isoelectronic $4d$ ion $Zr^{+}$. The $Os^{5}$+ form factor was found to give the best results, with both the $Ru^{5+}$ and $Zr^{+}$ form factors predicting an excessively shallow falloff of the magnetic intensity. The better match with the $Os^{5+}$ ion is unsurprising, given that the atomic radii differ by only $\sim 1$ pm. Sample fit and associated real space spin-spin correlation diagrams are shown in figure 7 for several temperatures between 45 K, just below $T_{N1}$, and 150 K. Below 45 K, the correlation length, as estimated from the full-width half maximum of the (100) peak, becomes larger than the maximum box sizes achievable.

Before discussing the results in Fig. 7, it is useful to consider the spin-spin correlations expected between various neighbors via the Goodenough-Kanamori (GK) rules[25,26]. The relevant geometric information is presented in Table 2. Most of the exchange pathways are of the super-super exchange (SSE) type as the intermediary diamagnetic ion, $Y^{3+}$, is involved. Considering just

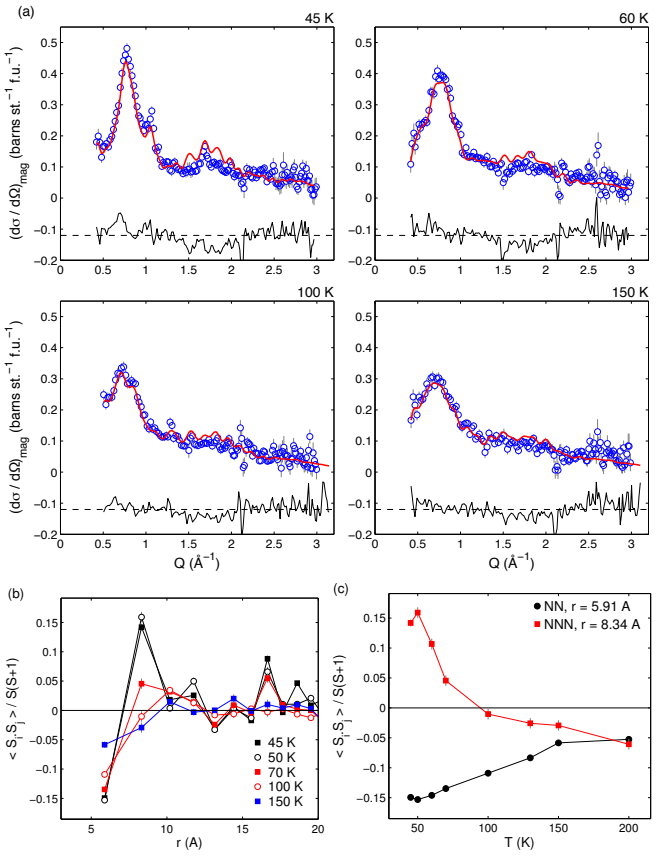


FIG. 7. (a) Results of an RMC analysis of diffuse magnetic scattering data for $Ba_2YRuO_6$ at $T = 45$, 60, 100, 150 K. Experimental points are open blue circles, with the fit and difference indicated by red and black lines, respectively. (b) Normalized spin-spin correlations $\langle S_i \cdot S_j \rangle / S(S+1)$ in direct space for several temperatures . (c) T-dependence of spin-spin correlations for the first two shells. Next nearest neighbor correlations cross over from antiferro- to ferromagnetic at $\sim$ 100 K.

TABLE II. Ru-Ru distances and exchange pathways in $Ba_2YRuO_6$, $a = 8.324$ Å.

| Neighbor ($z$) | Distance / Å | Pathway |
|---|---|---|
| $1^{st}$ (12) | 5.886 | 90° Ru-O-Y-O-Ru |
| $2^{nd}$ (6) | 8.324 | 180° Ru-O-Y-O-Ru |
| $3^{rd}$ (24) | 10.241 | complex |
| $4^{th}$ (12) | 11.827 | complex |

the first and second neighbors, for the nn case, there are two competing interactions, 90° $t_{2g}^3 - t_{2g}^3$ Ru-O-Y-O-Ru SSE, which is predicted to be weakly ferromagnetic (F), and direct $t_{2g}^3 - t_{2g}^3$ exchange which is antiferromagnetic (AF). While the Ru-Ru nn distances are long, given the enhanced radial extent of 4$d$ orbitals, a direct interaction cannot be ruled out absent a detailed calculation. Indeed, in some oxide materials the net interaction is AF.[25] The net sign of the nnn pathway should be less ambiguous; the 180° SSE is always AF in oxides. For example, in the $RE$CrO$_3$ ortho-perovskites ($RE$ = rare earth) in which the Cr-O-Cr angles are smaller than the ideal 180°, nnn SSE is AF and 120 K $< T_N <$ 280 K.[26] Thus, it is reasonable to expect that both nn and nnn interactions in $Ba_2YRuO_6$ are net AF. However, it also necessary to consider the demands of the Type I fcc magnetic structure shown in Fig. 2. It is clear the nn correlations involve 4 F and 8 AF correlations, while the nnn situation involves 6 F correlations. Thus, the Type I structure implies a severe compromise in terms of what might be expected given the exchange-pathway mandated correlations just discussed above.

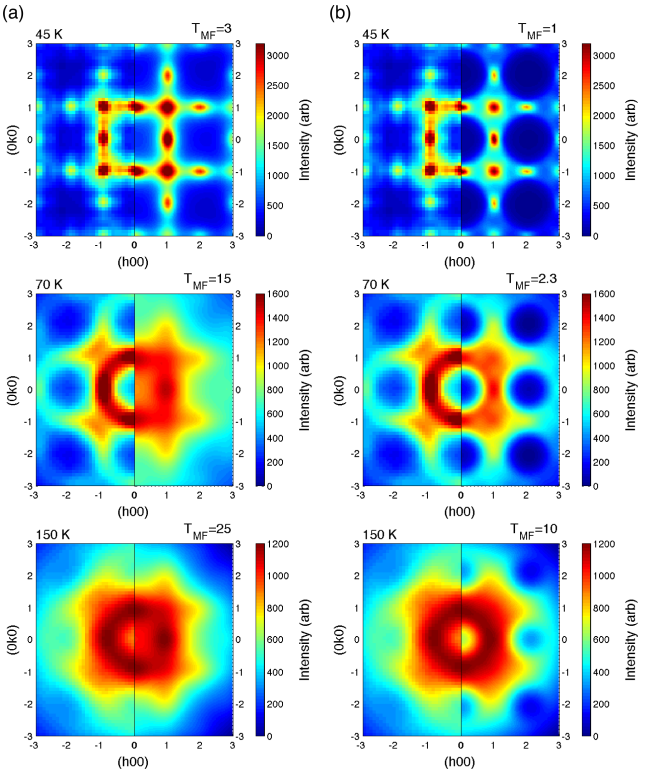


FIG. 8. Comparison between reconstructed single crystal scattering for $Ba_2YRuO_6$ (left half) and the mean field model (right half) described in the text. Exchange parameters for the latter were (a) $J_1 = -1$, $J_2 = -J_1/2$, $J_3 = 0$, $J_4 = 0$ and (b) $J_1 = -1$, $J_2 = 3J_1/8$, $J_3 = J_1/4$, $J_4 = 0$ .

Turning now to Fig. 7b, which displays the spin-spin correlation function $\langle S_i \cdot S_j \rangle$ at $T_{N2} = 45$ K, note that the spin correlations are exactly those expected for the Type I structure, *i.e.* net AF for nn and net F for nnn, which is of course required. The correlation length $\xi$ may be deduced to exceed 20 Å by comparing $\langle S_i \cdot S_j \rangle$ between pairs of sublattices at several distances. Regarding Fig. 7c, which shows the temperature dependence of $\langle S_i \cdot S_j \rangle$ for the first two coordination shells, a remarkable effect is observed on heating from 45 K; while the nn correlation remains AF at all temperatures, the nnn correlation changes sign by $\sim$ 100 K, roughly $2T_{N2}$, and becomes net AF at all higher temperatures. (Note

that $\langle S_i \cdot S_j \rangle$ at 16.6 Å falls to zero when the nnn value approaches zero.) This is the expected result based on the GK rules for the two shortest SSE pathways, and is of course consistent with the large negative value of the Curie-Weiss constant for $Ba_2YRuO_6$, $\theta_{CW} = -571$ K.

Can the RMC analysis provide insight regarding the detailed nature of the short range magnetic ordering in $Ba_2YRuO_6$ in direct space? For example, is there evidence for short-range $2D$ ordering near $T_{N1}$ as postulated for $Sr_2YRuO_6$? To this end, the $Q$-dependence of the single crystal diffuse scattering was reconstructed from the RMC fits using the SPINDIFF extension to SPINVERT. The $(hk0)$ scattering plane was chosen for this calculation, as a buildup of low dimensional correlations preceding magnetic order would manifest as rods or planes of scattering along the $(h00)$-type directions. Rod-like features are indeed observed in the reconstructed 45 K pattern, shown at the top of figure 8a, indicating the origin of the (100) peak broadening relative to (110) in the powder averaged data. To elucidate the dimensionality of the correlations when type I correlations are established, we calculated the $(hk0)$ magnetic scattering of Type I short-range order with anisotropic correlation lengths. This was done by writing the magnetic neutron cross section in terms of spin pairs

$$\left(\frac{d\sigma}{d\Omega}\right)_{mag} = C\mu f(Q)^2 \left[\frac{2}{3} + \frac{1}{N}\sum_{i,j} \hat{\mathbf{S}}_i^{\perp} \cdot \hat{\mathbf{S}}_j^{\perp} \cos \mathbf{Q} \cdot \mathbf{R}_{ij}\right], \tag{2}$$

where $\hat{\mathbf{S}}^{\perp}_{(i,j)}$ are the components of normalized spins $i$ and $j$ perpendicular to $\mathbf{Q}$, and $\mathbf{R}_{ij}$ is the vector connecting them, and then making the substitution

$$\hat{\mathbf{S}}_i^{\perp} \cdot \hat{\mathbf{S}}_j^{\perp} = \exp\left[-|R_{ij}^z|/\xi_z - \sqrt{(R_{ij}^x)^2 + (R_{ij}^y)^2}/\xi_{xy}\right], \tag{3}$$

where $\xi_z$ ($\xi_{xy}$) are the correlation lengths along and perpendicular to $\mathbf{k} = \{(100), (010), (001)\}$. Evaluating the resulting expression numerically for boxes of spins of dimension $\gg \xi_z(\xi_{xy})$ and for all three $\mathbf{k}$-domains leads to the right hand side of figure 9. In the top half, $\xi_z = 25.2$ Å and $\xi_{xy} = 4.2$ Å is considered, whereas the lower panel shows $\xi_z = 8.4$ Å and $\xi_{xy} = 16.8$ Å; the parameter sets selected are both roughly compatible with the average correlation length extracted from the full width half maximum of (100). Qualitative agreement with the data at 45 K is good for the former scenario, *i.e.* essentially $1D$ antiferromagnetic correlations. This is in sharp contrast to the interpretation of the diffuse scattering in [16], where the asymmetric line-shape of the (100) reflection in Q was thought to reflect 2D correlations. The ferromagnetic correlations $\perp$ $\mathbf{k}$ manifest as rods for (h00) and (0k0) odd, and are also observed at 45 K. On heating further, these rods first disappear, before the pattern becomes more isotropic beyond 70 K (Figure 8).

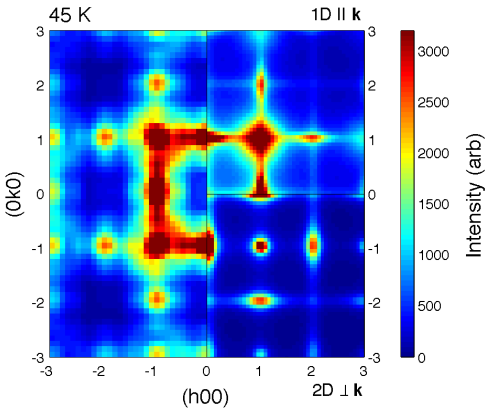


FIG. 9. Comparison between the $(hk0)$ plane scattering reconstructed from the RMC fits to 45 K data (left) and the numerically evaluated scattering in the same plane for (right, upper) domains with $\xi_z = 25$ Å and $\xi_{xy} = 4.2$ Å, and (right, lower) domains with $\xi_z = 8$ Å and $\xi_{xy} = 16$ Å.

We finally attempt to establish the connection between the diffuse scattering in the $(hk0)$ plane and the exchange parameters of the system by way of a mean field model[27–29]. The Hamiltonian for this model may be written

$$\mathcal{H} = -\frac{1}{2}\sum_{i,j} J_{ij}(\mathbf{R}_{ij})\mathbf{S}_i \cdot \mathbf{S}_j, \tag{4}$$

where $S_i$ and $S_j$ are classical Heisenberg spins on sites $i, j$ connected at distance $|\mathbf{R}_{ij}|$ by $J_{ij}(\mathbf{R}_{ij})$ (note the sign of the exchange). We have chosen to cut the latter off at a distance of 12 Å, corresponding to the fourth coordination shell. The spectrum of eigenvalues of this Hamiltonian, corresponding to the various possible classical magnetic structures, may be determined by first Fourier transforming, then diagonalizing the interaction matrix $J_{ij}(\mathbf{q})$, where $\mathbf{q}$ is a vector in the first Brillouin zone. The ground state is the mode which maximizes $J(\mathbf{q})$, and hence minimizes Eq. 2. Using the eigenvalues and eigenfunctions determined in this way, the scattering cross section for $T > T_{N2}$ may be written:

$$\left(\frac{d\sigma}{d\Omega}\right)_{mag} = Cf(Q)^2 \sum_{\eta,\alpha} \frac{\left|F^{\eta}_{\perp,\alpha}\right|^2}{3 - \lambda^{\eta}_{\mathbf{q}}/T_{MF}} \tag{5}$$

where $\mathbf{Q} = \mathbf{q}+\mathbf{G}$, with $\mathbf{G}$ a reciprocal lattice vector. The superscript and subscript labels denote the $\alpha = (x, y, z)$ spatial components of eigenvalue $\lambda$ of index $\eta$. $T_{MF}$ is the mean field temperature of the calculation, here treated as an adjustable parameter. The so-called mean-field structure factor in the numerator is

$$F^{\eta}_{\perp,\alpha}(\mathbf{Q}) = F^{\eta}_{\alpha}(\mathbf{Q}) - \hat{Q}_{\alpha}\left[\sum_{\beta} \hat{Q}_{\beta} F^{\eta}_{\beta}(\mathbf{Q})\right] \tag{6}$$

where $\hat{Q}_{(\alpha,\beta)}$ are unit vectors along $\alpha, \beta = (x, y, z)$. Finally, the $Q$-dependent part is

$$F_\alpha^\eta(\mathbf{Q}) = \sum_i u^\eta_{\mathbf{q};i,\alpha} \exp(-i\mathbf{G}\cdot\mathbf{R}_i) \quad (7)$$

where $u^\eta_{\mathbf{q};i,\alpha}$ is the $\alpha$ component of the eigenvector on site $i$ associated with eigenvalue $\lambda^\eta$, and the sum runs over all atoms in the asymmetric unit. The general features of the scattering *i.e.* the rods of scattering perpendicular to (100) and the differing T-dependences of the (100) and (110) peaks are well reproduced for nearly all solutions with antiferromagnetic nn coupling $J_1$ and ferromagnetic nnn coupling $J_2$ [Figure 8a]. As expected, these solutions correspond to the stability criterion for the Type I structure. Some features, such as the ring of scattering evident at low $Q$ in the high $T$ calculated patterns, and the absence of scattering at (110) above 70 K, are however less well described by these solutions. To ensure that these differences are not a consequence of the RMC parameters, we reconstructed the ($hk0$) scattering for a variety of box sizes and weights. As we found relatively little variation with respect to these, the discrepancy between the $J_1$-$J_2$ is likely due to other interactions in the system; here, we focus on further neighbor couplings.

By including an antiferromagnetic $3^{rd}$ neighbor coupling $J_3$ and changing the sign of $J_2$ to antiferromagnetic (in accordance with the GK prediction) both the low $Q$ ring and the form of the scattering at larger $Q$ are well reproduced [Figure 8b]. The change of sign of $J_2$ is furthermore consistent with the negative antiferromagnetic nnn correlations observed in our RMC fits at high temperature. Again, multiple solutions for $J_3 > 0$ and $J_2 > 0$ give acceptable agreement with the data; in figure 8, we show a comparison between the parameter set $J_1 = -1$, $J_2 = 3J_1/8$, $J_3 = J_1/4$, $J_4 = 0$ and the experimental data. Although $J_2 < 0$ favors Type II order, it is negated by a relatively small $J_3 < 0$, which has a strong effect by virtue of the large number of neighbors $z$.

To place the comparison between the Monte-Carlo and mean field datasets on a more quantitative footing, we compute a quality factor $\chi^2 = \sum_{\mathbf{q}}[\sigma_{rc}(\mathbf{q}) - \sigma_{mf}(\mathbf{q})]^2$, where $\sigma_{rc(mf)}$ denote the reconstructed and mean field cross sections for each set of parameters. The solution with $J_3 \neq 0$ yields a lower $\chi^2$ at all $T$; at 45 K, $\chi^2$ for the $J_3 \neq 0$ set is 7.6, while $J_3 = 0$ yields 8.7. This difference increases to 10.4 ($J_3 \neq 0$) versus 31 ($J_3 = 0$) at 70 K. While this strongly suggests the presence of interactions beyond $J_2$, powder averaging makes it difficult to distinguish between the $J_3 \neq 0$ model and other scenaria, including ring exchanges and anisotropies. As such, an accurate microscopic picture will likely require an actual measurement of the ($hk0$) plane from a single crystal, ideally with energy analysis. Nonetheless, the foregoing treatment (as well as [22]) illustrates how RMC can provide surprisingly detailed information on 3D spin arrangements in disordered magnetic systems.

## III. SUMMARY AND CONCLUSIONS.

Using polarized neutrons, the magnetic scattering cross section for the highly frustrated double perovskite $Ba_2YRuO_6$ has been measured from 1.8 K to 200 K over the range $0.4 < Q < 3.85$ Å$^{-1}$. The Type I fcc magnetic structure is confirmed at low temperatures with two apparent orderings at $T_{N2} \sim 36$ K and $T_{N1} \sim 47$ K. Near $T_{N2}$ the (100) magnetic reflection broadens significantly while the (110), (210), (211), (300) and (310) peaks remain apparently Bragg-like until $T_{N1}$. The widths of the (110) and (210) reflections broaden continuously between $T_{N2}$ and $T_{N1}$ indicating the presence of short range spin correlations within this interval. These results are parallel to those reported for monoclinic $Sr_2YRuO_6$ for which $T_{N2}$ and $T_{N1}$ are 27 K and 32 K, respectively. Diffuse magnetic scattering associated with the (100) feature persists up to at least 200 K, $\sim 6T_{N2}$. Again, $Sr_2YRuO_6$ shows a similar effect. Unlike for $Sr_2YRuO_6$, however, the peak shape of the diffuse feature at $Q_{100} = 0.75$ Å$^{-1}$ is not obviously either an asymmetric Warren or a symmetric Lorentzian function.

Below $T_{N1}$, a drastic decrease in the integrated intensity is observed, ascribed to a gap in the spin excitations, which opens at this temperature in inelastic measurements [15]. A gap of comparable magnitude must be responsible for similar behavior in $Sr_2YRuO_6$. Analysis of the diffuse magnetic scattering above and slightly below $T_{N1}$ was carried out using reverse Monte Carlo (RMC) methods to yield information on the spin-spin correlations in direct space. By reconstructing the ($hk0$) plane scattering from the RMC spin configurations, it was found that the correlations in this range are predominantly one-dimensional and antiferromagnetic, with the 2D correlations growing on cooling below $T_{N1}$. In addition, comparison of the calculated ($hk0$) plane with mean field calculations shows that a complete model of $Ba_2YRuO_6$ likely requires couplings beyond nn and nnn. This may also be the case for most other double perovskites of this type, including $Sr_2YRuO_6$. Application of the Goodenough-Kanamori rules indicate that both the nn and nnn couplings should be AF, however, for $T < 2T_{N2}$, the nnn correlation is F. This can be understood in terms of the further neighbor couplings identified by the mean field calculation. A more detailed study on both the diffuse scattering and dynamics in the ordered phase, ideally on a single crystal, will probably be required to unambigusouly determine the microscopic Hamiltonian. Electronic structure calculations would prove a useful supplement to these experiments.

## ACKNOWLEDGMENTS

We acknowledge very useful discussions with B.D. Gaulin and E. Kermarrec, and J. P. Carlo for discussions and providing his inelastic neutron scattering data. J.E.G. thanks the Natural Sciences and Engineering Re-

search Council of Canada for support via a Discover Grant. G.J.N. is grateful to McMaster University for hospitality during a one month residence. G.E. acknowledges funding by the Scientific User Facilities Division, Office of Basic Energy Sciences, U.S. Department of Energy.

## Appendix A

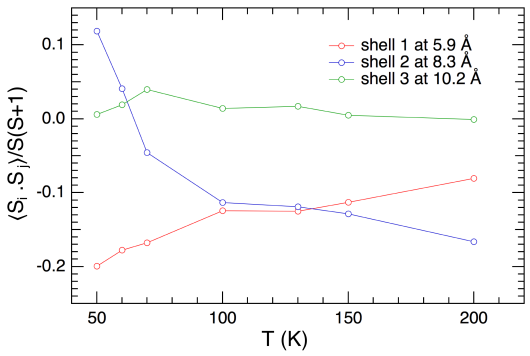


FIG. 10. Normalized spin-spin correlations $\langle S_i \cdot S_j \rangle / S(S+1)$ versus $T$ calculated from spin configurations obtained using an alternate code. The sign and magnitude of the nn correlations are well reproduced, while the nnn correlations tend on average slightly more towards antiferromagnetism.

Fits to the data from 50 K to 200 K were also carried out using the locally developed code of G. Ehlers.[30] There was generally good agreement between this approach and SPINVERT as indicated by Figure A1. The only significant difference is that the cross-over in $\langle S_i \cdot S_j \rangle$ from F to AF for nnn occurs at $\sim 70$ K rather than $\sim 100$ K.

* Email address: nilsen@ill.fr


[1] V. M. Goldschmidt, Naturwissenschaften **14**, 477 (1926).
[2] C. J. Howard, B. J. Kennedy, and P. M. Woodward, Acta. Cryst. B **59**, 463 (2003).
[3] G. Chen, R. Pereira, and L. Balents, Phys. Rev. B **82**, 174440 (2010).
[4] G. Chen and L. Balents, Phys. Rev. B **84**, 094420 (2011).
[5] T. Dodds, T.-P. Choy, and Y. B. Kim, Phys. Rev. B **84**, 104439 (2011).
[6] F. E. Mabbs and D. J. Machin, Magnetism and Transition Metal Complexes (Chapman and Hall, 1973) p. 93.
[7] C.-G. Ma and M. G. Brik, J. Lumin. **145**, 402 (2014).
[8] E. E. Rodriguez, F. Poineau, A. Llobet, B. J. Kennedy, M. Avdeev, G. J. Thorogood, M. L. Carter, R. Seshadri, D. J. Singh, and A. K. Cheetham, Phys. Rev. Lett. **106**, 067201 (2011).
[9] J. Mravlje, M. Aichhorn, and A. Georges, Phys. Rev. Lett. **108**, 197202 (2012).
[10] P. D. Battle and W. J. Macklin, J. Solid State Chem. **52**, 138 (1984).
[11] P. D. Battle and C. W. Jones, J. Solid State Chem. **78**, 108 (1989).
[12] T. Aharen, J. E. Greedan, F. Ning, T. Imai, V. Michaelis, S. Kroeker, H. D. Zhou, C. R. Wiebe, and L. M. D. Cranswick, Phys. Rev. B **89**, 134423 (2009).
[13] S. Middey, A. K. Nandy, S. K. Pandey, M. P., and D. D. Sarma, Phys. Rev. B **86**, 104406 (2012).
[14] H. Matsuura and K. Miyake, J. Phys. Soc. Japan **82**, 073703 (2013).
[15] J. P. Carlo, J. P. Clancy, K. Fritsch, C. A. Marjerrison, G. E. Granroth, J. E. Greedan, H. Dabkowska, and B. D. Gaulin, Phys. Rev. B **88**, 024418 (2013).
[16] E. Granado, J. W. Lynn, K. F. Jardin, and M. S. Torikachvili, Phys. Rev. Lett. **110**, 017202 (2013).
[17] R. P. Singh and C. V. Tomy, Phys. Rev. B **78**, 024432 (2008).
[18] J. R. Stewart, P. P. Deen, K. H. Andersen, H. Schober, J. F. Barthelemy, J. M. Hillier, A. P. Murani, T. Hayes, and B. Lindenau, J. Appl. Crystallogr. **42**, 69 (2009).
[19] O. Schaerpf and H. Capellmann, Phys. Status Solidi A **135**, 359 (1993).
[20] N. G. Parkinson, P. P. Hatton, J. A. K. Howard, C. Ritter, F. Z. Chien, and M.-K. Wu, J. Mater. Chem. **13**, 1468 (2003).
[21] Y. Jiang, A. Huq, C. Booth, G. Ehlers, J. E. Greedan, and J. S. Gardner, J. Phys.: Condens. Matter **23**, 164214 (2011).
[22] J. A. M. Paddison and A. L. Goodwin, Phys. Rev. Lett. **108**, 017204 (2012).
[23] J. A. M. Paddison, J. R. Stewart, and A. L. Goodwin, J. Phys.: Condens. Matter **25**, 454220 (2013).
[24] K. Kobayashi, T. Nagao, and M. Ito, Acta Cryst. A **67**, 473 (2011).

[25] J. Kanamori, J. Chem. Phys. Solids **10**, 87 (1959).
[26] J. B. Goodenough, Magnetism and the Chemical Bond (Interscience, 1963) pp. 169–183.
[27] J. N. Reimers, Phys. Rev. B **46**, 193 (1992).
[28] H. Kadowaki, Y. Ishii, K. Matsuhira, and Y. Hinatsu, Phys. Rev. B **65**, 144421 (2002).
[29] M. Enjalran and M. J. P. Gingras, Phys. Rev. B **70**, 174426 (2004).
[30] Details available on request.